Coupled variability and air-sea interaction in the South Atlantic Ocean

Andreas Sterl, Wilco Hazeleger

Royal Netherlands Meteorological Institute (KNMI)

P.O. Box 201, NL-3730 AE De Bilt, Netherlands

phone: +31-30-2206766; fax: +31-30-2202570; e-mail: sterl@knmi.nl

ABSTRACT

52 years of data (1949-2000) from the NCEP-NCAR reanalysis are used to investigate mechanisms involved in forcing and damping of Sea Surface Temperature (SST) variability in the South Atlantic Ocean. Organized patterns of coupled ocean-atmosphere variability are identified using EOF and SVD analyses. The leading mode of coupled variability consists of an SST pattern with a strong northeast-southwest gradient and an SLP monopole centered at 15°W, 45°S. The anomalous winds associated with this monopole generate the SST pattern through anomalous latent heat flux and mixed layer deepening. Other heat flux components and anomalous Ekman transport play only a secondary role. Once established, the SST pattern is attenuated through latent heat flux. The higher SST modes are also induced by anomalous winds and destroyed by latent heat flux. It thus appears that the coupled variability in the South Atlantic Ocean consists of atmospheric circulation anomalies that induce SST anomalies through anomalous latent heat fluxes and wind-induced mixed layer deepening. These SST anomalies are destroyed by latent heat flux with no detectable systematic feedback onto the atmospheric circulation. Atmospheric variability in the South Atlantic is found to be largely independent of that elsewhere, although there is a weak relation with ENSO (El Niño-Southern Oscillation).

1 Introduction

Climate variability on longer than annual time scales is believed to arise from an interplay of ocean and atmosphere. Both the ocean and the atmosphere transport energy and exchange it with each other. The dynamics of both systems are thus coupled via exchange processes at their common interface. To understand climate variability it is vital to study the common variability of both systems and its relation to the exchange processes.

While a vast amount of studies have been devoted to the coupled variability of ocean and atmosphere in the North Atlantic (e.g., Kushnir 1994, Deser and Blackmon 1993, Grötzner et al. 1998), the South Atlantic has got little attention. However, the South Atlantic is unique in transporting energy *towards* the equator, forming an important link in the Global Ocean Conveyor (Gordon 1986). Ocean-atmosphere interaction in this basin may thus have implications for other areas of the Globe, especially the North Atlantic region, which lies downstream on the Conveyor. However, due to the slow propagation of disturbances in the ocean modifications of the Conveyor originating in the South Atlantic would impact the Northern Hemisphere only on a longer time scale (e.g., Weijer et al. 2002).

The tropical Atlantic is known to influence North Atlantic climate on shorter time scales through the atmosphere. Robertson et al. (2000) have found a connection between SST variability in the tropical South Atlantic and that of pressure over the North Atlantic region. Similar conclusions have been arrived at by Okumura et al. (2001) and Ruiz-Barradas et al. (2000),

while Sutton et al. (2000) find that the North Atlantic Oscillation (NAO) acts as a forcing for SST variability in the tropical Atlantic. Xie and Tanimoto (1998) describe a pan-Atlantic SST pattern reaching from South Africa to Greenland.

Most studies on Atlantic variability, including those just mentioned, only consider the area north of about 30°S. They find a large SST (sea surface temperature) signal in the eastern tropical Atlantic (e.g., Ruiz-Barradas et al. 2000, Sutton et al. 2000), which is related to changes (position and strength) of the Trade Wind system. If the southern boundary of the domain is situated further south, an additional SST signal in the southwestern part of the basin emerges that is related to atmospheric circulation anomalies as evidenced by SLP (sea level pressure) (Venegas et al. 97, Wainer, Venegas 2002) or 200 hPa winds (Robertson, Mechoso 2000).

Venegas et al. (1997 and 1998; hereafter VMS97 and VMS98, respectively) have studied the covariability of SST and SLP in the South Atlantic (equator to 50°S). While in VMS98 they concentrate on longer time scales, inter-annual timescales are considered in VMS97. They use 40 years of data from COADS (Woodruff et al. 1987), from which they identify three coupled modes of variability with periods of ≈ 14-16 years, ≈ 6-7 years and ≈ 4 years, respectively, accounting for nearly 90% of the total squared covariance. The third mode (4 years, 6%) is found to be strongly correlated with the El Niño-Southern Oscillation (ENSO) phenomenon.

In the present paper we use the NCEP/NCAR reanalysis data (Kalnay et al. 1996) to study the mechanisms behind coupled ocean-atmosphere variability in the South Atlantic. Reanalysis results can be considered as model output constrained by observations. Being model output the data is internally consistent, while the incorporation of observations guaranties that they reflect the real climate system. We use SST and SLP as the basic variables describing the ocean and the atmosphere, respectively. These variables are linked with each other through processes at the air-sea interface like surface heat fluxes. These fluxes are also available from the reanalysis data and are used here to identify the processes that are important for the generation and attenuation of SST anomalies. Growth and decay of such anomalies depend not only on the atmospheric forcing, but also on oceanic processes which in turn depend on oceanic properties. Due to the lack of oceanic data, some crude assumptions have to be made to account for the ocean's role in creating SST variability. This leads to a form of the SST-tendency equation in which all terms can be estimated from the reanalysis data. This equation is used to study the mechanisms of the coupled variability in the South Atlantic. Using statistical methods (EOF and SVD analyses) we first identify and describe the main patterns of coupled and uncoupled surface variability in the South Atlantic Ocean, answering the question of *how* the system varies. The results are broadly consistent with those of VMS97. We then turn to our main question which is *why* it varies by relating the growth and decay of SST anomalies to the different forcing mechanisms.

2 Dataset description and preparation

2.1 Data

In this study we use data from the NCEP/NCAR reanalysis (Kalnay et al. 1996). We define the South Atlantic to be the area between 50°W and 20°E and between 45°S and the equator. The western limit at 50°W excludes the highly variable Brazil/Malvinas Confluence Region near 45°S, 55°W. While the leading variability patterns are unaffected by this rather local phenomenon, it tends to dominate the higher modes that explain less variability. Their patterns are rather localized and do not describe basin-wide variability. Therefore we exclude this region from our analysis. The southern and eastern limits of the domain are chosen as to keep the domain as small as possible to study variability in the South Atlantic only. Extending the domain to the south and to the east yields dominant patterns of variability that are either identical to those obtained for the smaller domain, or that do not have a signal within that domain. The choice

of the equator as the northern boundary is somewhat arbitrary. However, using 45°N instead did not change the results. The leading patterns of SST and SLP found on this larger domain encompass those presented in section 2.3 for the South Atlantic domain alone. In particular, the first EOF of SLP found on the larger domain is solely confined to the Northern Hemisphere, while the second EOF equals our first one. For SST, our first EOF is the southern part of the first EOF obtained for the whole Atlantic. The latter spans the whole basin and is the same pattern that Dommenget and Latif (2000) found in the GISST data set.

The NCEP/NCAR reanalysis covers the period from 1949 until now. For this work we have used the 52 years from 1949 to 2000. Due to data-sparseness, the quality of the reanalysis is questionable before 1958, while it should be much higher than on average during the most recent years when the introduction of satellites tremendously increased the amount of data to be assimilated. We therefore repeated our analyses with data for different sub-periods (1958-2000, 1980-2000). These analyses gave essentially the same results as those presented here for the full 1949-2000 period.

Throughout the paper monthly-mean data are used. Monthly-mean anomalies are calculated by subtracting from each individual monthly mean the long-term mean of the corresponding calendar month. A possible linear trend is also removed. The results presented in this paper were derived using all calender months. Using only data from one calendar month (say, May) did not change the results very much. The EOF and SVD patterns derived for individual calendar months are very similar to those obtained for all months, and the corresponding time series are highly correlated.

2.2 Quality of reanalysis data

In a reanalysis, observed SST is specified as the lower boundary condition for an integration of an atmospheric general circulation model (AGCM) which is constrained by assimilating all available meteorological observations (mainly wind, pressure, and air temperatures). Every 6 hours the atmosphere model is "pushed" towards these observations in a way not violating physical laws. A reanalysis is thus forced to follow the observed variability of the atmosphere. This makes a reanalysis differ from an AMIP-type integration, in which the AGCM is unconstrained and free to follow its own variability.

The extent to which the AGCM in the reanalysis is constrained depends on the amount of data available. In the South Atlantic Ocean data density is much lower than for the oceans in the Northern Hemisphere. This could raise concerns that in this ocean the reanalysis run would have many characteristics of an AMIP-type run. AMIP-type runs are known to produce unrealistic heat fluxes of even the wrong sign because the fixed SST implies an infinite heat content of the ocean (Barsugli and Battisti 1998). However, although observations were sparse during the early years of the reanalysis, the South Atlantic never was observation-void. There are shipping lanes from South America and South Africa to Europe and North America. The route around the Cape of Good Hope is particularly well visible between 1967 and 1975, when the Suez Canal was closed. Furthermore, there are a few Islands (St. Helena, Ascension, Gough, ...) with weather stations, which unfortunately only came into operation during the 1970s. With the introduction of satellites during the 1980s, observation density in the South Atlantic has increased dramatically.

Evidence for the realism of the variability exhibited by the reanalysis comes from an investigation into the relation between latent heat flux and the change of SST, $\partial_t T_s$. In the extratropics these two quantities are expected to be highly correlated (e.g., Cayan 1992). Sterl (2001b) showed that this correlation is present in the reanalysis data throughout the whole period and has the correct sign, i.e., SST is warming (cooling) for heat flux entering (leaving) the ocean. The correlation becomes much stronger after 1981, when the SST data improved due to

the availability of satellite data.

That the reanalysis does not simply reflect the atmosphere model's internal variability can also be seen from correlations between results from the NCEP-NCAR reanalysis and the ERA15 reanalysis. For zonal wind stress the correlations exceeds 0.9 for most of the South Atlantic (Sterl 2001b), while for the less constrained latent heat flux it still exceeds 0.6 (Sterl 2001a,b). If the reanalyses just displayed the internal variability of the respective AGCMs, such large correlations would not be expected.

Correlations only measure the *phase* of the variations, leaving open the possibility of *amplitudes* being systematically wrong. To investigate into this, we compared the variances of the NCEP/NCAR flux-anomalies with those of other flux data sets. We tried the new ECMWF reanalysis, ERA40, the COADS-based Da Silva (Da Silva et al. 1994) dataset, and the satellite-based HOAPS (Graßl et al. 2000) dataset. Compared to ERA40, the NCEP/NCAR variability appears to be larger, especially in the north-eastern part of the basin. The differences are larger in the earlier years than they are in the most recent periods. In regions of good data coverage, i.e., along the shipping lanes, the variability of NCEP/NCAR is larger than that from Da Silva, while it is much smaller in data-sparse regions. Finally, the NCEP/NCAR variability is smaller, in a large region even much smaller, than that found in HOAPS. These results are equivocal as to whether the NCEP/NCAR fluxes overestimate the true fluxes. We therefore think that it is justifiable to use the reanalysis' flux data, all the more as no alternative exists.

Besides SST, which is imposed as the lower boundary condition, all reanalysis quantities are model output and therefore automatically internally consistent. This property is important when one wants to study the interplay between different quantities, e.g., the coupled variability of ocean and atmosphere. Sterl (2001a) has shown that in data-sparse areas datasets purely based on observations do not necessarily possess this property, which may lead to erroneous results about the covariability of different quantities.

2.3 Description of South Atlantic variability

We now come to the description of the leading patterns of variability of SST and SLP in the South Atlantic Ocean. To do so, we first perform Empirical Orthogonal Function (EOF) analyses of SST and SLP and then turn to their coupled variability by performing a combined Singular Value Decomposition (SVD) analysis of the two quantities. These analyses result in patterns and time series. The latter are often called Principal Components (PCs). The actual anomaly described by a specific EOF or SVD is given by the product of pattern and time series. Only this product has a physical meaning. Thus pattern and PC can be scaled arbitrarily, as long as their product remains the same. We here adopt a scaling such that the PCs have unit variance, so that the patterns represent a typical anomaly. Only the patterns are presented in the following.

The results largely resemble those of VMS97. Nevertheless, we discuss them shortly as the patterns are used when determining mechanisms of SST variability in section 4.

2.3.1 EOF analysis of SST and SLP

Figure 1 shows the patterns of the two leading EOFs of SST with climatological SST superimposed. The first EOF nearly vanishes in the south-western part of the domain, but has its signal in the area where the climatological SST has a gradient pointing to the northwest, i.e., along a line stretching from South Africa to northwest Brazil. This is the path of the South Equatorial Current, the equatorward flowing part of the subtropical gyre. The EOF acts to shift the region of maximum SST gradient along that current, acting to warm/cool it. The second EOF has its center near 20°W, 30°S. In this region the climatological isotherms are nearly zonal, and the EOF describes their north/south shift in a large area of the southwestern South Atlantic.

Figure 2 shows the patterns of the first two EOFs of SLP with the climatological SLP
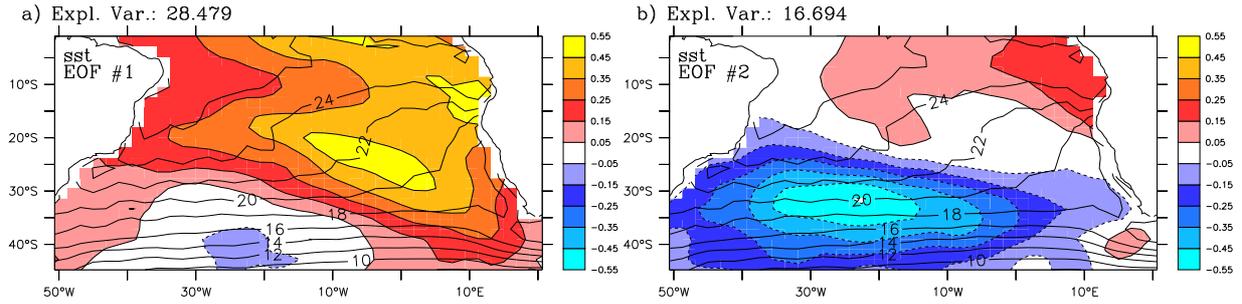
Figure 1: *Patterns of the first two EOFs of SST anomalies (colours, in K) with the climatological SST superimposed (contours, in °C). Explained variance is displayed on top of each panel.*
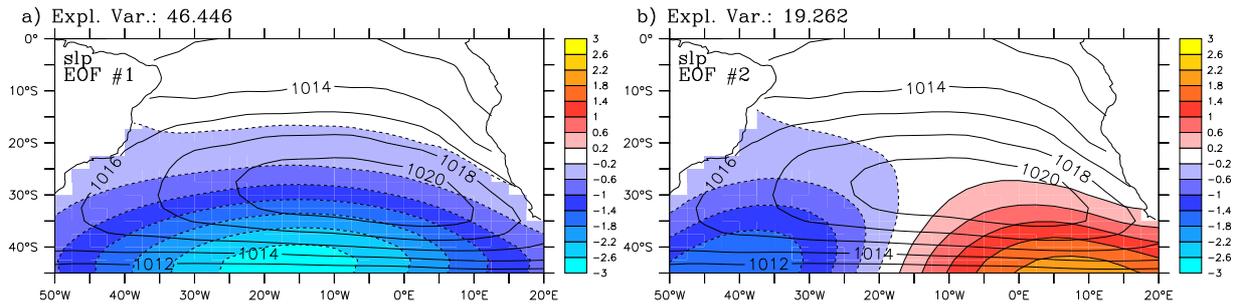
Figure 2: *Patterns of the first two EOFs of SLP anomalies (colours, in hPa) with the climatological pressure superimposed (contours, in hPa). Explained variance is displayed on top of each panel.*

superimposed. By far the most variance (46%) is explained by the first EOF, representing a monopole centered at 15°W, 45°S. It describes a weakening and north-south displacement of the climatological subtropical high, thereby changing the predominantly westerly winds along $\approx$ 35°S. The second EOF describes an east-west displacement of the same subtropical high. However, caution is needed in interpreting this EOF. Its pattern suggests an anticorrelation between SLP in the eastern and the western part of the basin which does not show up in the raw data (not shown). EOF analysis is designed to maximize the explained variance of a pattern. As Dommenget and Latif (2002) have pointed out, this may lead to linearly independent variability being squeezed into one EOF with a higher EOF being needed to correct for this. Therefore, the second EOF is likely to be an artifact of the EOF technique.

The spectra of the principal components (not shown) conform to expectations: Those of SST are red, and those of SLP are nearly white. The only significant peak on interannual times scales is one at about 5 years in the first PC of SST, while a second peak at about 13 years fails to reach the 95% significance limit. SLP exhibits no significant peaks on interannual time scales.

The EOF patterns found here are broadly consistent with those obtained by VMS97, who used different datasets and did not detrend their data prior to doing the EOF analysis. The common features are that both analyses reveal that the largest SST signal is in the northeastern part of the basin, and the second largest in the southwestern part. However, the partition of these signals between the EOFs is different. In both analyses, the largest SLP signal is found to be a monopole having its center near the southern edge of the domain.

Performing EOF analyses of SLP on larger domains (e.g., whole circumpolar ocean) reveals the same structures as found here to describe the variability in the South Atlantic (not shown). They can thus be regarded as the South Atlantic expression of circumpolar variability. It is,
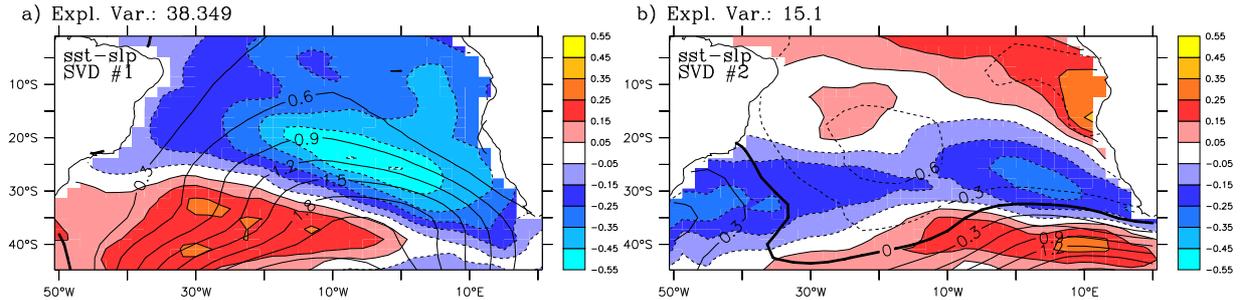
Figure 3: *First two leading modes of a combined SVD analysis of anomalies of SST (colours, in K) and SLP (contours, negative contours dashed, in hPa).*

however, worth pointing out that the variability in the South Atlantic basin is largely independent of the variability elsewhere. Correlations between SLP at a point somewhere in the South Atlantic (e.g., at the centre of our first EOF) and SLP in the whole Southern Hemisphere are small outside the South Atlantic basin. A significant pole of opposite polarity is found in the South Indian Ocean, but the correlation there does not exceed 0.35.

2.3.2   Combined SVD analysis of SST and SLP

To investigate the combined variability of ocean and atmosphere we perform a maximum covariance analysis on SST and SLP using Singular Value Decomposition (SVD). This technique searches for modes that explain as much as possible of the mean-squared temporal covariance between the two fields (Bretherton et al. 1992).

Figure 3 shows the first two SVD modes. Clearly, there is a close correspondence between the respective first EOF patterns (see Figures 1a and 2a) on one side and the first SVD patterns on the other. Furthermore, the first PCs of the SVDs and those of the corresponding EOFs are highly correlated and their spectra are almost identical (not shown). For the second SVD mode the correspondence with the respective EOFs is much lower, although the corresponding PCs are still significantly correlated. The dissimilarity between the second SLP SVD and the second SLP EOF may be taken as additional evidence for the second EOF to be an artifact of the analysis technique.

From Figure 3 it is obvious that the maxima of SST coincide with regions in which the pressure has a large gradient. This suggests that the occurrence of SST anomalies might be related to changes in wind or wind stress. This idea is further investigated in section 4, where we try to identify mechanisms that force the main variability patterns described so far into existence, as well as those that destroy them.

3   Forcing and damping of surface variability

3.1   The SST equation

After having identified preferred patterns of coupled ocean-atmosphere variability we want to investigate causes and effects of their development. As SST is a key quantity in relating ocean and atmosphere, we will concentrate on the question of how SST anomalies are generated and how they are destroyed. To do so, we consider the different terms in the SST tendency equation

$$\partial_t T_s = -\vec{v} \cdot \nabla T_s - \frac{Q}{h\rho_w c_p} + D. \tag{1}$$

The SST, T_s, is assumed to equal the temperature of the surface mixed layer of depth h. Furthermore, $\rho_w \approx 1000$ kg/m^3 is the density and $c_p \approx 4 \cdot 10^3$ W kg^{-1} K^{-1} is the specific heat of water. Q is the total surface heat flux leaving (cooling) the ocean, $\vec{v}$ is the velocity in the upper layer of the ocean, and D represents diffusive terms. In the following we discuss these terms in more detail and indicate how we can estimate them from the reanalysis data.

3.1.1 Heat flux

The total heat flux Q can be decomposed into respectively latent, sensible, long-wave, and short-wave flux,

$$Q = Q_{lat} + Q_{sens} + Q_{lw} + Q_{sw}. \tag{2}$$

The sum of latent and sensible heat is also referred to as turbulent heat flux (Q_{turb}), and the sum of long and short wave flux as radiative flux (Q_{rad}). The reanalysis data contain these terms separately.

3.1.2 Advection

The total velocity $\vec{v}$ in (1) can be decomposed into the Ekman velocity that is locally generated by the wind stress $\vec{\tau} = (\tau_x, \tau_y)$, and the pressure (density) driven geostrophic part ($\vec{v}_g$). Lacking ocean current data, only the Ekman part can be considered here. However, inspection of the ocean reanalysis performed by Carton et al. (2000a,b) reveals that the currents in the upper ocean are dominated by the Ekman currents.

The horizontal components $\vec{u}_e = (u_e, v_e)$ of the Ekman velocity are that part of the total velocity that balance the surface stress (e.g., Gill 1982, pp 320/321). The resulting expression is singular at the equator, where the Coriolis parameter f vanishes. This singularity can be avoided by adding linear friction $-r\,\vec{u}_e$ to the governing equations (Zebiak and Cane 1987). Doing so, the Ekman transport (= vertically integrated velocity) is given by

$$\vec{U}_e = (U_e,\, V_e) = \frac{1}{\rho_w(f^2 + r^2)}\left(f\tau_y + r\tau_x,\; -f\tau_x + r\tau_y\right). \tag{3}$$

For $r = 0$ the usual form of the Ekman transport is retrieved. Following Zebiak and Cane (1987), we use a value of $r = 0.5$ d^{-1}, which is small enough to be negligible away from the equator, but large enough to avoid the singularity. Requiring the Ekman transport to be divergence free yields the vertical or Ekman pumping velocity

$$w_e = \nabla \cdot \vec{U}_e = \frac{1}{\rho_w(f^2 + r^2)}\left(f\,(\nabla \times \vec{\tau})_z + r\,\nabla \cdot \vec{\tau}\right). \tag{4}$$

The SST equation (1) then becomes

$$\partial_t T_s = -\frac{1}{h}\left(\vec{U}_e \cdot \nabla_h T_s + \mathsf{H}(w_e)w_e\Delta T + \frac{Q}{\rho_w c_p}\right) + \vec{v}_g \cdot \nabla T_s + D, \tag{5}$$

where ∇_h is the horizontal part of the gradient operator and ΔT is the temperature jump across the base of the mixed layer. The Heaviside function H appears in (5) because vertical transport will only influence the mixed layer temperature if it is directed upward, bringing colder water into the mixed layer.

3.1.3 Mixing

The diffusive term D describes the effect of horizontal and vertical mixing of water masses. Near the surface vertical mixing is much more important than horizontal mixing, as horizontal

temperature gradients are much smaller than the vertical ones. The latter can reach large values at the base of the surface mixed layer, where temperature jumps of 1-2 K can occur. Mixing that water into the surface mixed layer has a great impact on SST, especially when the mixed layer is shallow. The effect of vertical mixing on SST depends not only on the atmospheric forcing (buoyancy loss and wind stirring), but also on the vertical density structure of the ocean. As we lack data on the latter, we have to make some additional assumptions to quantify the impact of mixed layer deepening on SST. Rather than to provide exact numbers, the following discussion is therefore only meant to estimate the importance of wind stirring on SST changes relative to other processes.

For this discussion we use the framework of a bulk mixed layer model as introduced by Niiler and Kraus (1977) and applied to an Ocean General Circulation Model by, e.g., Sterl and Kattenberg (1994). Mixed layer deepening can occur through buoyancy loss at the surface with subsequent convection, through velocity shear, and through wind-stirring. Except for very high latitudes, where SST is very low, and tropical regions with high precipitation, salinity effects on density are small, so that buoyancy loss is mainly proportional to heat loss. Therefore, its effect on SST is at least partly captured by the heat flux term in (5). The effect of velocity shear is small and mainly proportional to the wind stirring term (Sterl and Kattenberg, 1994). The latter is proportional to the third power of the friction velocity u_*, which itself is defined by $u_*^2 = \tau/\rho_w$. In a purely wind-driven situation the bulk mixed layer equation reduces to

$$m_1 u_*^3 e^{\frac{-hf}{0.4u_*}} - \frac{1}{2} \partial_t h \, \Delta b \, h = 0, \tag{6}$$

where Δb is the jump of specific buoyancy $b = -g(\rho_w - \rho_0)/\rho_0$ across the base of the mixed layer, ρ_0 being a reference density and g the gravitational acceleration, and m_1 is a tunable parameter, for which Sterl and Kattenberg (1994) recommend a value of 2. For mixed layer depths between 50 and 100 m as considered here, the product $m_1 \exp[(-hf)/(0.4u_*)]$ is thus of order one. Using this value yields

$$\partial_t h = \frac{2u_*^3}{h\Delta b} \tag{7}$$

for the rate of mixed layer deepening. Assuming that density is only governed by temperature, the buoyancy jump is given by

$$\Delta b = g \, \gamma \, \Delta T, \tag{8}$$

where $\gamma \approx 0.2 \cdot 10^{-3} \ \text{K}^{-1}$ is the thermal expansion coefficient of water of about 14°C. Note that the value of γ varies by a factor of three between 4°C and 25°C (Gill 1982, Table A3.1).

Heat is conserved when the mixed layer deepens from h to $h + \Delta h$. This leads to

$$\partial_t T_s|_{\text{mix}} = -\frac{\partial_t h}{h + \Delta h} \Delta T \tag{9}$$

for the change of SST due to vertical mixing. Neglecting Δh in the denominator of (9) and inserting (7) and (8) finally yields

$$\partial_t T_s|_{\text{mix}} = -\frac{2u_*^3}{h^2 g \gamma} = -\frac{\alpha}{h^2} u_*^3, \tag{10}$$

which is independent of ΔT. As ΔT increases, less but colder water is entrained into the mixed layer (i.e., $\partial_t h$ decreases) to achieve the same change in temperature. The factor $\alpha = 2/(g\gamma) \approx 10^3 \ \text{Ks}^2\text{m}^{-1}$ depends on the precise values of γ and m_1, which are not known. The value of 10^3 only gives an order-of-magnitude. Based on the variation in γ and the uncertainty of m_1, an uncertainty of a factor of two seems realistic for α. Inserting (10) into (5) yields

$$\partial_t T_s = -\frac{1}{h} \left(\vec{U}_e \cdot \nabla_h T_s + \mathsf{H}(w_e) w_e \Delta T + \frac{Q}{\rho_w c_p} + \frac{\alpha u_*^3}{h} \right) + \vec{v}_g \cdot \nabla T_s + D', \tag{11}$$

where D' represents those mixing terms not accounted for by (10).

3.2 Evaluation of terms

The horizontal Ekman heat transport $\vec{U}_e \cdot \nabla_h T_s$ in (11) can be calculated from the NCEP-NCAR reanalysis data. As monthly-mean values for both $\vec{U}_e$ and $\nabla_h T_s$ are used, sub-monthly variations in advective heat transport are neglected. Sub-monthly effects may be important in regions of large variability as the Cape Basin, were Agulhãs rings enter the South Atlantic, or in the vicinity of the equatorial currents. The vertical transport cannot be calculated thoroughly, as ΔT is unknown. We assume that T decreases with depth and use a constant ΔT of 2 K. This value is representative for most of the basin but might be too low for the region of the Angola-Benguela Front off the Namibian coast. Here warm and saline Angola Current water from the north is situated above cold and less saline water from the Benguela current (Lass et al. 2000). By taking ΔT constant, the "re-emergence" mechanisms (e.g., Alexander and Deser 1995), by which temperature anomalies are temporarily shielded from the surface by a shallow summer mixed layer, cannot be taken into account. Running an ocean model is needed to study this effect.

The mixed layer depth h is also unknown in (11). We derived a monthly climatology of h from the ocean reanalysis described by Carton et al. (2000a,b). We defined h as the depth at which the temperature deviates by more than 0.5 K from SST. We use a climatological mixed layer depth rather than the actual values as the Carton et al. (2000a,b) reanalysis uses wind stress from Da Silva et al. (1994). As shown in Sterl (2001a) the variability of this wind stress product differs significantly from that of the NCEP/NCAR reanalysis. As mixed layer depth is governed largely by the wind stress, the Carton et al. (2000a,b) mixed layer depth therefore might not be compatible with the results of the NCEP/NCAR reanalysis. However, using a monthly climatology of h includes the effects of spatial variation as well as the annual cycle. Especially the latter has a significant impact on the results. The quantity u_*^3 has been calculated from daily values of $\vec{\tau}$ and thus contains the effect of intra-monthly variability.

The derivation leading to (11) is valid for the full variables. However, we will apply the equation to monthly anomalies by subtracting the mean annual cycle as described in section 2. To do so, we decompose each term in (11) into mean and anomaly, but we do not do so for each factor separately. For instance, we consider the anomaly of $\vec{U}_e \cdot \nabla_h T_s/h$, but not that of $\vec{U}_e$ or $\nabla_h T_s$, and only the mean annual cycle of h is taken into account. For anomalies defined this way, (11) is equally valid. Unless otherwise noted, only these monthly anomalies are considered in the remainder of this paper. For notational convenience, they are denoted by the same symbols as used above for the full quantities without primes or other distinguishing symbols being added. Likewise, we will speak of, for instance, "heat flux" instead of "anomalies of heat flux".

3.3 Relative importance of forcing terms

To asses the relative importance of the forcing terms in (11) we calculate the local regression coefficient between $\partial_t T_s$ and the forcing terms. Let (a, b) be an inner product between two time series a and b. Then $\mathrm{corr}(a, b) = (a, b)[(a, a)(b, b)]^{-1/2}$ is the correlation, and $\mathrm{reg}(a, b) = (a, b)/(a, a)$ is the regression between the two series. As the former is normalized by the standard deviations of the two series it does not contain information on amplitudes or relative importance. This information is contained in the regression. Note, however, that $\mathrm{reg}(a, b) \neq \mathrm{reg}(b, a)$.

The SST tendency equation (11) has the form $\partial_t T_s = a + b + c + ...$ Regressing each term of this equation on $\partial_t T_s$ yields

$$1 = \mathrm{reg}(\partial_t T_s, \partial_t T_s) = \mathrm{reg}(\partial_t T_s, a) + \mathrm{reg}(\partial_t T_s, b) + \mathrm{reg}(\partial_t T_s, c) + ... \qquad (12)$$

Each term on the right-hand side of this equation measures the contribution of the respective forcing term to $\partial_t T_s$, i.e., its relative importance. In principle, some of the regression coefficients
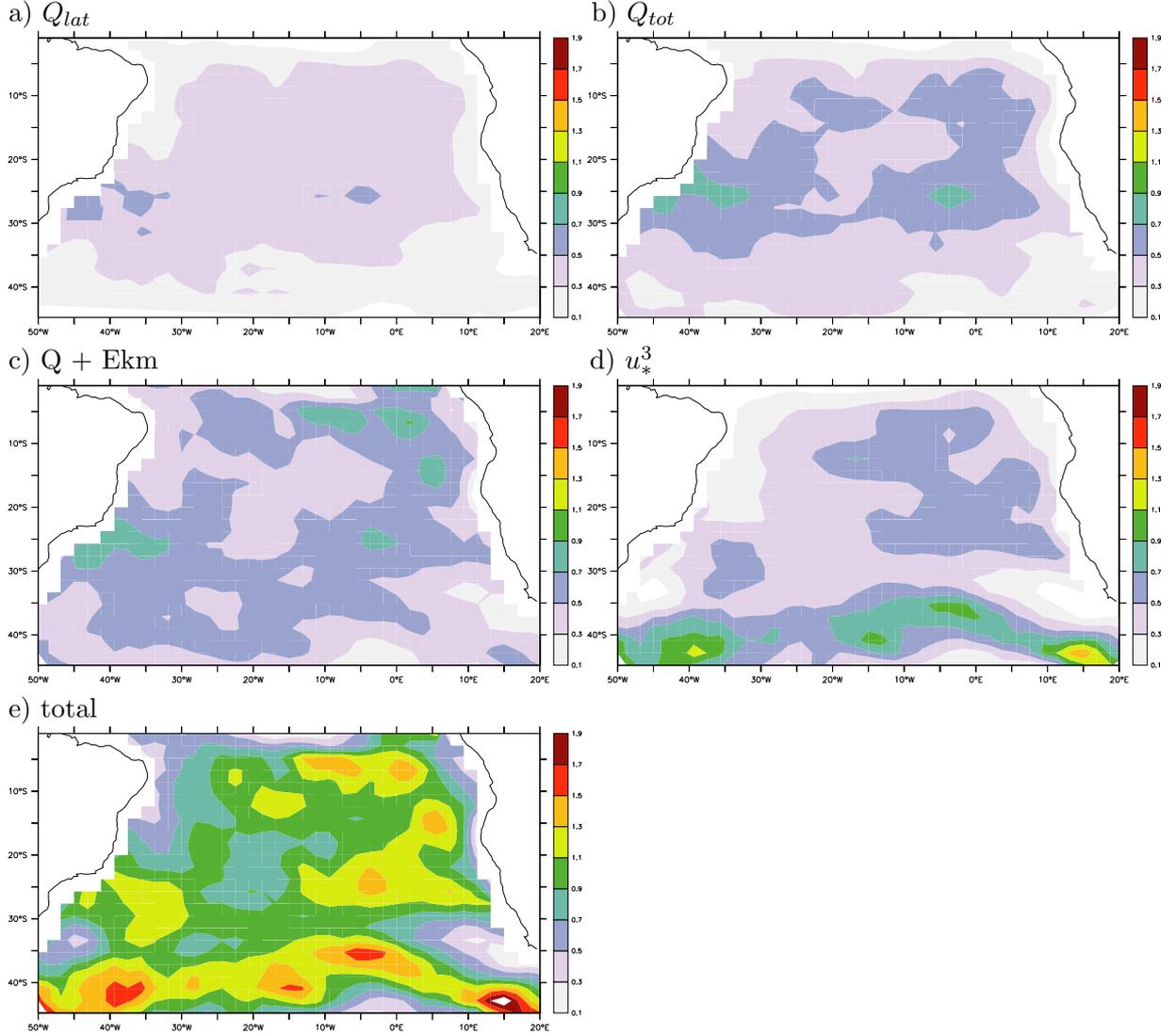
Figure 4: *Local regression of $\partial_t T_s$ anomalies on anomalies of different forcing fields as given in (11): a) Q_{lat}, b) Q, c) sum of Q and Ekman terms, d) wind stirring, and e) total resolved forcing (sum of c) and d)). All factors (including the sign) appearing in (11) are accounted for, with h taken from the results of Carton et al. (2000a,b) as explained in the text.*

can become negative. In that case an SST anomaly would develop *against* a counteracting forcing. However, this does not happen in the South Atlantic (see Figure 4).

The results of this exercise are displayed in Figure 4. The regressions between SST change and latent heat flux display values between 0.3 and 0.5 (Figure 4a) in most of the domain. This means that Q_{lat} accounts for $\approx 40\%$ of the changes in SST. Adding the other heat flux components generally increases the regression to values around 0.6 (Figure 4b), i.e., their contribution is less than one-third of that of latent heat flux. Figure 4c, in which the Ekman terms are added to the heat flux, shows that the former are much smaller than the latter throughout the domain. Finally, the regression between SST change and wind stirring (Figure 4d) is comparable to that for total heat flux (Figure 4b) except poleward of 40°S. In the "Roaring Forties" the importance of wind mixing for SST change by far exceeds that of heat flux.

Adding the contributions from all forcings considered yields values around or slightly exceeding unity for most parts of the domain (Figures 4e). Thus heat flux, Ekman temperature

transport and wind-induced mixing explain most of the SST changes, especially if we take the uncertainties due to the use of a climatological mixed layer depth, the value of α in (10), and a constant value for ΔT into account. In one region this is not true, namely in the small region near the southern tip of Africa that shows up as having low values in Figure 4e. Here, warm Agulhãs rings enter the relatively cold South Atlantic, which may make the geostrophic advection term in (11) important.

Due to the lack of ocean data, the above reasoning gives only a rough approximation of the relative importance of different forcing mechanisms. A more realistic assessment can only be done if more high-quality observational data of the upper ocean were available, or through modeling. It *can* be said, however, that surface heat flux Q is more important than Ekman transports, that latent heat flux is much more important than the other heat flux components, that meridional Ekman transport is more important than the zonal one (not shown), and that wind-induced mixing is as important as surface heat flux. Additional tests using only data from one particular calendar month showed that these general conclusions hold regardless of season.

4 Life cycle of SST anomalies

4.1 Lagged regressions between SST patterns and atmospheric circulation

To get more insight into the temporal evolution of the anomaly patterns described in section 2.3, we now present sequences of lagged regression patterns between the PCs of the SST SVDs and quantities describing the coupled evolution of oceanic and atmospheric anomalies, namely SST, SLP, and wind stress. This is done in Figure 5. At lag zero, one can recognize the SVDs presented before. At negative lags, i.e., at times preceding the maximum of the patterns considered, we see how they gradually built up over ≈ 6 months. Likewise, the destruction of the anomalies takes ≈ 6 months, too. This timescale of about half a year is consistent with the e-folding time of the auto-correlation function of the SST PCs (not shown). Based on this e-folding time and a corresponding reduction in the degrees-of-freedom, a t-test reveals (not shown) that regression values exceeding ≈ 0.15 K (SST) or ≈ 15 hPa (SLP) are significant at the 95%-level.

Figure 5 shows a clear relation between SST anomalies and wind stress anomalies during the built-up phase, with maximum wind stress anomalies appearing over areas of maximum SST anomalies. During the destruction phase, such a relation is less apparent, if not absent. This suggests that wind (or wind stress) plays a forcing role in generating SST anomalies, but not in destroying them, meaning that SST changes do not feed back on the atmospheric circulation in a systematic way. Wind (stress) can affect SST through several mechanisms, namely by enhancing the latent heat flux, by inducing currents that advect SST anomalies, and by inducing vertical mixing that deepens the mixed layer.

4.2 Lagged regressions between SST SVDs and forcing fields

We now investigate the role of the different forcings according to (11) leading to the life cycle of anomalies just described. To do so, we follow the method employed in the foregoing subsection by lag-regressing the PCs of the different SVDs onto the full anomalous forcing fields. As we use regression rather than correlation, all fields can be compared directly with one another, making it possible to assess their relative importance. As in Figure 5, the developing SST anomalies are used as a background on which the regressions of the forcing fields are plotted, making it easy to identify coinciding SST/forcing patterns.

To start with, Figure 6 shows the regressions of the principal component of the SST SVDs on SST (colours) and total heat flux (contours). According to (11) the heat flux is related to the change of SST, not to SST itself. Therefore the patterns have no direct physical meaning, but
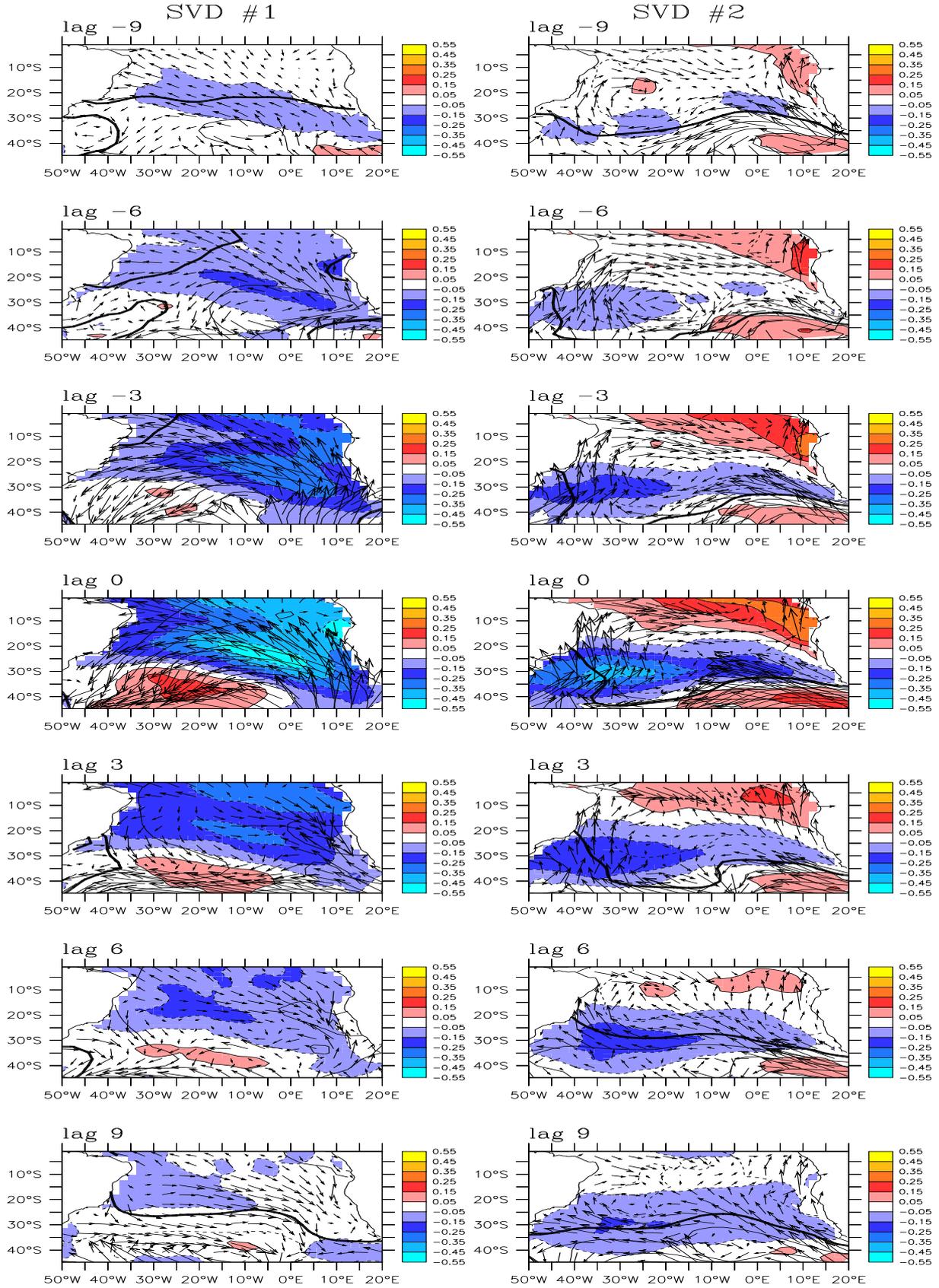
Figure 5: *Sequence of lagged regressions of anomalies of SST (colours, in K), SLP (contours, spacing = 10 hPa), and wind stress (arrows) on the PCs of the SST SVDs from Figure 3. Lag is positive when the PC leads.*
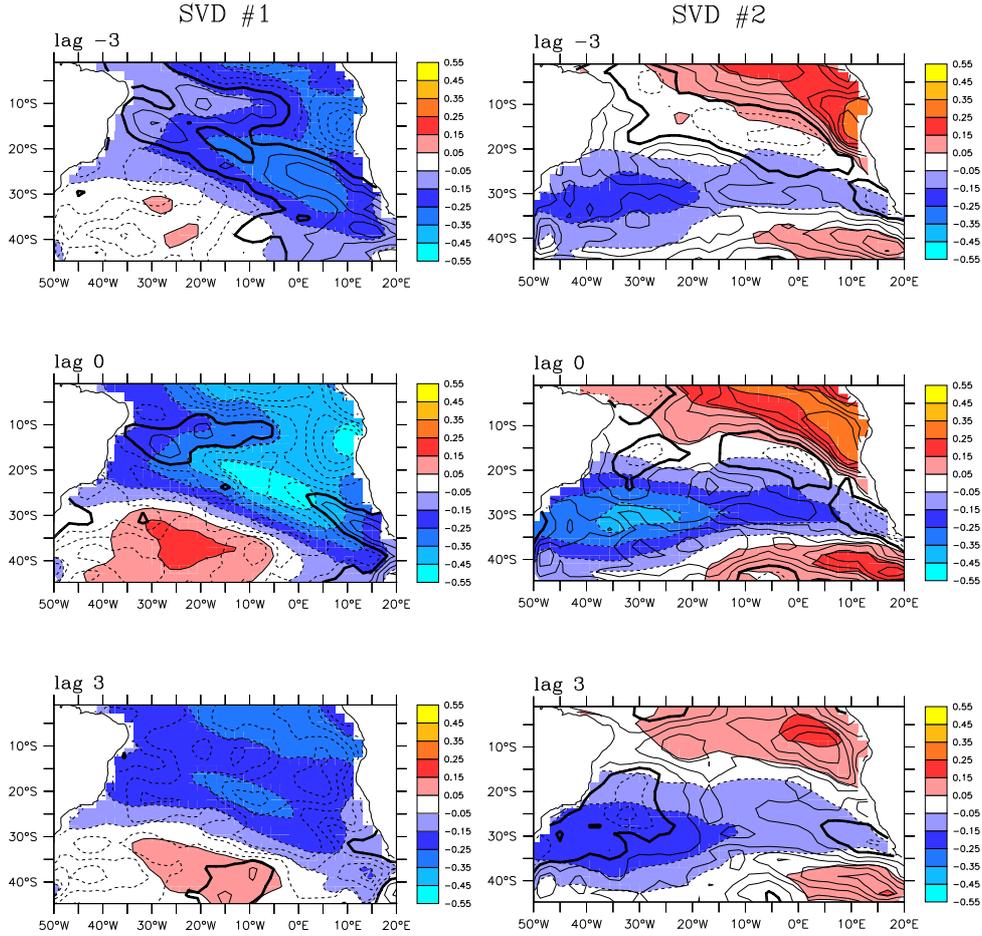
Figure 6: *Sequence of lagged regressions of anomalies of SST (colours, in K) and total heat flux* $(-Q/(\rho_w\, c_p))$, *contours, spacing* $= 3 \cdot 10^{-7}$ *Km/s) on the PCs of the SST SVDs from Figure 3.* *Lag is positive when the PC leads.*

they show whether the heat flux acts to enhance or to damp the SST anomalies. As a positive heat flux cools the ocean, the heat flux damps the SST anomalies if both have the same sign, and forces them if the signs are opposite. For SVD-1 opposite signs at negative lags occur over most of the domain, most notably in the South Equatorial Current, where this SVD has its maximum signal. For SVD-2 forcing occurs in the southwestern part of the basin, also a region of maximum signal. At lag 0 and at positive lags, heat flux is damping the SST anomlies. Thus in both cases the heat flux acts to *create* the SST anomaly (opposite sign of SST and heat flux anomaly at negative lags), but helps to destroy it after it has reached its maximum (equal signs at positive lags). Splitting the total heat flux up into its different components reveals that the latent heat flux is by far the most important one. The corresponding regression patterns look almost as those obtained for the total heat flux (not shown).

For SVD-1 the patterns of heat flux and SST in the South Equatorial Current region coincide for several months. The heat flux thus systematically forces the SVD-1 SST pattern there. A comparison with Figure 5 shows that in the same region also the anomalous wind (stress) reaches its maximum. The latter is directed northwestward, enforcing the climatological wind that can be inferred from the climatological SLP shown in Figure 2. The anomalous wind has two impacts on the heat flux. Firstly, it increases the advection of cold air from the southeast into the region in question, and secondly, it increases the wind speed. Both changes increase the turbulent heat

13
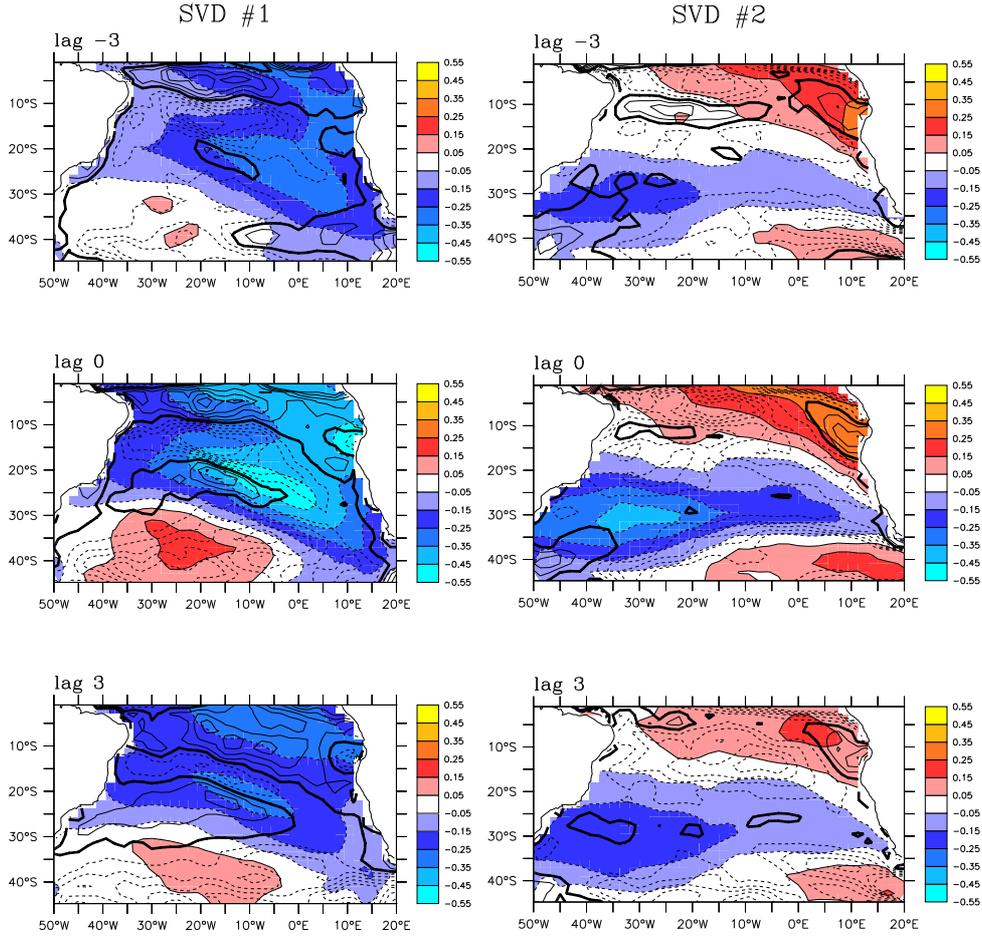
Figure 7: *Sequence of lagged regressions of anomalies of SST (colours, in K) and meridional Ekman heat transport (contours, spacing = $1 \cdot 10^{-7}$ Km/s) on the PCs of the SST SVDs from Figure 3. Lag is positive when the PC leads.*

loss. Thus the anomalous heat flux forcing of the SVD-1 pattern is caused by an anomalous atmospheric circulation.

As has been shown in section 3.3, heat flux in the extra-tropics is dominated by latent heat flux. Roughly speaking, it is proportional to the product of wind speed, U, and $\Delta q_{sa} = q_s - q_a$, where q_a is the specific humidity of the air and q_s the saturation humidity for air of temperature T_s. Decomposing both factors into mean and anomaly leads to

$$Q'_{lat} \sim (U \, \Delta q_{sa})' = \overline{U} \, \Delta q'_{sa} + U' \, \overline{\Delta q_{sa}} + U' \, \Delta q'_{sa}, \tag{13}$$

where the overbar denotes the mean and the prime the anomaly. As q_s is monotonously increasing with SST, a positive (negative) SST anomaly will usually lead to a positive (negative) anomaly of Δq_{sa}. The observed damping of SST anomalies by heat flux is thus mainly caused by the first term in (13). As we argued in the discussion above, parts of the SST anomaly described by the first SVD are forced by wind-induced heat flux anomalies, i.e., the terms involving U' in (13). A regression of the PCs onto these terms confirms that view. Paraphrasing, $U' \, \overline{\Delta q_{sa}}$ forces SST anomalies, while $\overline{U} \, \Delta q'_{sa}$ damps them.

Calculating the lagged regressions for the other terms in (11) confirms the earlier finding that in general both Ekman heat transport and Ekman pumping (Figures 7 and 8, respectively) are at least a factor of three smaller than heat flux (note the smaller contour interval). However,

14
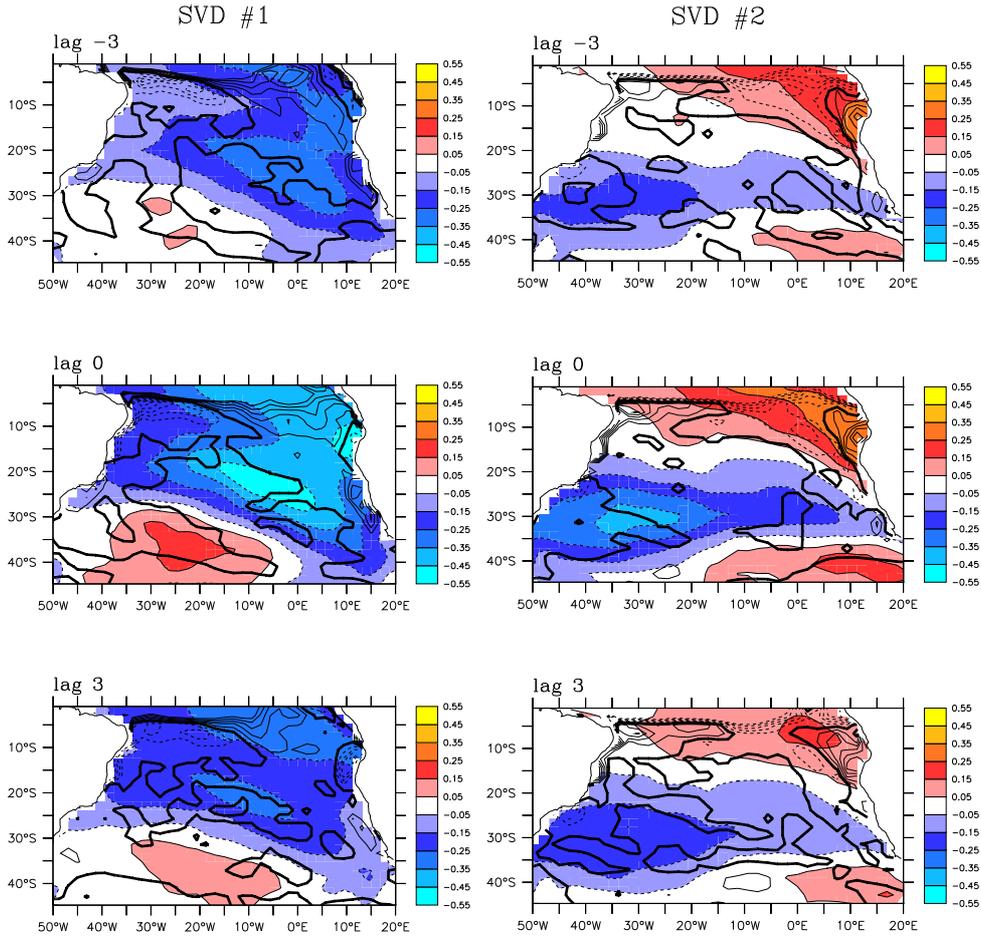
Figure 8: *Sequence of lagged regressions of anomalies of SST (colours, in K) and Ekman pumping ($\Delta T = 2$ K, contours, spacing $= 1 \cdot 10^{-7}$ Km/s) on the PCs of the SST SVDs from Figure 3. Lag is positive when the PC leads.*

both of them act, at least partly, to create the anomalies described by the SVDs. Ekman pumping helps to enforce the anomalies of both SVDs in the northeastern part of the basin. Except for the regions just mentioned, the relation between Ekman pumping and Ekman heat transport on the one hand and the SST SVDs on the other is not obvious.

Finally, Figure 9 shows the relation between the SST SVDs and the wind-mixing term in (11). As in the analysis of section 3.3, the magnitude of the wind forcing is comparable to that of heat flux. Furthermore, wind-induced mixing always generates the SST patterns. This is most clearly seen for SVD-1. In SVD-2, the regions of maximum SST anomaly and maximum wind stirring are displaced relative to one another. However, also heat flux and Ekman heat transport contribute to the creation of this pattern. The contribution of wind-stirring to the destruction of SST anomalies is generally small and not systematic. Only the first SVD experiences some systematic damping by mixed layer dynamics, but it is smaller than that caused by heat flux (compare the two lag-3 panels of Figures 6 and 9).

Anomalous wind-stirring is also related to anomalous wind speed, and the correlation coefficient between u_*^3 and $U'\overline{\Delta q_{sa}}$ has values of around 0.9 in the South Atlantic Ocean. A plot of the relation between the SST SVDs and $U'\overline{\Delta q_{sa}}$ analogous to Figure 9 (not shown) reveals that both mechanisms are equally important in creating the first SVD. However, unlike u_*^3, $U'\overline{\Delta q_{sa}}$ contributes neither to the creation of the second SVD nor to the destruction of the first in any systematic way.
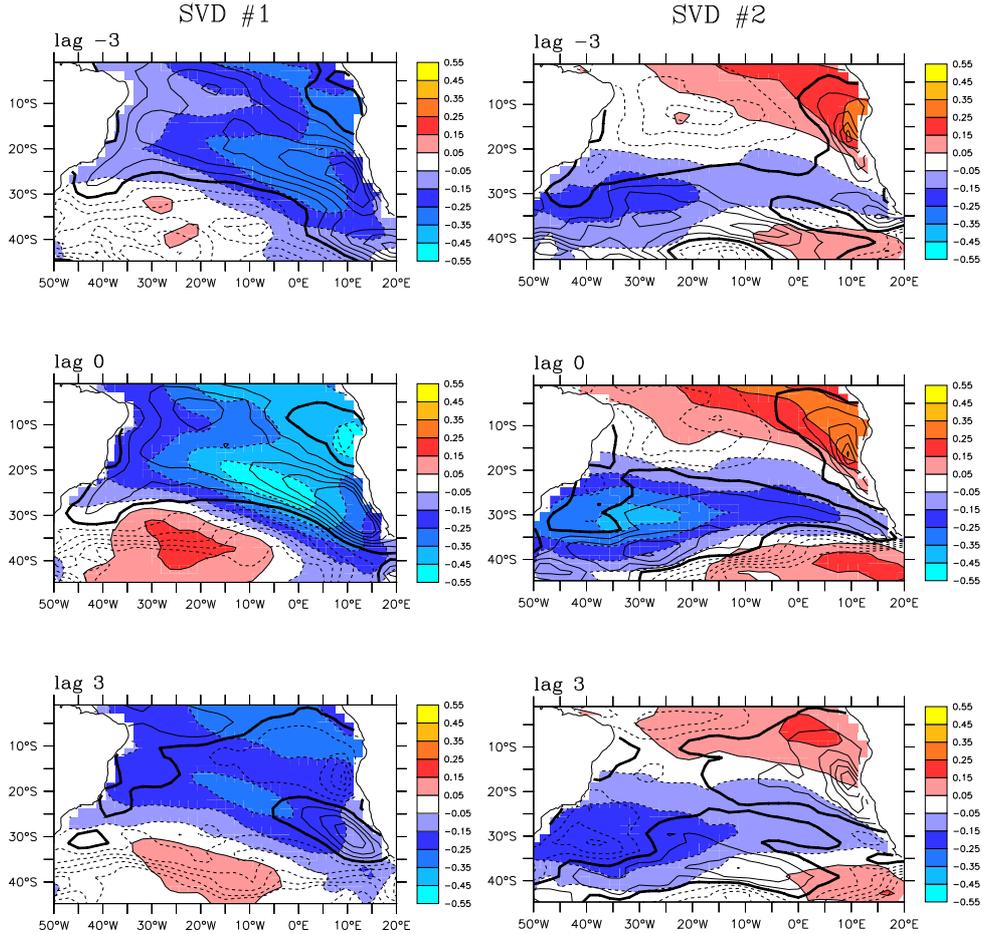
Figure 9: *Sequence of lagged regressions of anomalies of SST (colours, in K) and wind stirring ($-\alpha\, u_*^3$, contours, spacing $= 3 \cdot 10^{-7}$ Km/s) on the PCs of the SST SVDs from Figure 3. Lag is positive when the PC leads.*

Concluding, SST anomalies are mainly wind-induced. The largest contributions come from changes in wind-induced mixed-layer deepening and wind-induced latent heat flux ($U' \overline{\Delta q_{sa}}$) and smaller ones from changes in Ekman heat transport and Ekman pumping. The decay of SST anomalies is caused by the heat flux, which is dominated by the latent heat flux. The damping is mainly accomplished by the term $\overline{U}\, \Delta q'_{sa}$.

5 Summary and Conclusion

The coupled ocean-atmosphere variability in the South Atlantic Ocean on time scales of months to years has been investigated using 52 years of data (1949-2000) from the NCEP/NCAR re-analysis (Kalnay et al. 1996). The main mode of coupled variability consists of a dipole SST pattern that resembles a plane inclined from the northeast to the southwest and a corresponding SLP pattern that changes the predominantly westerly winds along $\approx 35°$S. This mode of SLP variability is part of the large variability that occurs in the circumpolar Southern Ocean. However, the variability in the South Atlantic Ocean is largely independent of the variability elsewhere in the Southern Ocean and even in the rest of the world. Specifically, no relation with the North Atlantic Oscillation was found, and only a weak one with ENSO (second SVD; not shown, but in accordance with VMS97).

16

The main mechanism for generating large-scale SST anomalies in the South Atlantic Ocean appears to be atmospheric variability. Anomalous winds associated with atmospheric pressure anomalies generate SST anomalies through anomalous latent heat flux and mixed layer deepening. The other heat flux components as well as Ekman transports play only a minor role. Changes in latent heat flux are brought about both by changes in wind speed and anomalous atmospheric heat advection. Once established, SST anomalies are damped by latent heat flux. There is no detectable feedback of SST anomalies on the atmospheric circulation.

More data sets as well as modeling are needed to answer open questions. The ERA40 reanalysis currently being performed at ECMWF will provide one such dataset. Ocean modeling is needed to provide the necessary information on oceanic processes like heat advection and mixed layer deepening in generating and destroying SST anomalies. In the present analysis, the role of these processes could be assessed only indirectly, and several additional assumptions had to be made. Finally, to investigate how the interplay between oceanic and atmospheric processes leads to coupled variability, coupled models are needed.

6   References

Alexander, M.A., and C. Deser (1995) A mechanism for the reoccurrence of wintertime midlatitude SST anomalies, *J. Phys. Oceanogr.,* **25**, 122-137.

Barsugli, J.J., and D.S. Battisti (1998) The basic effects of atmosphere-ocean thermal coupling on mid- latitude variability, *J. Atmos. Sci.,* **55**, 477-493.

Bretherton, C.S., C. Smith, J.M. Wallace (1982) An intercomparison of methods for finding coupled patterns in climate data, *J. Clim,* **5**, 541-560

Carton, J.A., G. Cherupin, X. Cao, and B. Giese (2000a) A simple ocean data assimilation analysis of the global upper ocean 1950-1995. Part I: Methodology, J. Phys. Oceanogr., **30** 294-309

Carton, J.A., G. Cherupin, X. Cao, and B. Giese (2000b) A simple ocean data assimilation analysis of the global upper ocean 1950-1995. Part II: Results J. Phys. Oceanogr., **30** 311-326

Cayan, D.R. (1992) Latent and sensible heat flux anomalies over the Northern Oceans: Driving the sea surface temperature, *J. Phys. Oceanogr.,* **22**, 859-881.

Da Silva, A.M., C.C. Young, and S. Levitus (1994) Atlas of surface marine data. Vol. 1, Algorithms and procedures, *NOAA Atlas Series,* **6**, 74 pp, NOAA, Washington, D.C.

Deser, C., and M.L. Blackmon (1993) Surface climate variations over the North Atlantic Ocean during winter: 1900-1989, *J. Clim.,* **6**, 1743-1753.

Dommenget, D., and M. Latif (2000) Interannual to decadal variability in the tropical Atlantic, *J. Climate* **13**, 777-792.

Dommenget, D., and M. Latif (2002) A cautionary note on the interpretation of EOFs, *J. Climate* **15**, 214-225.

Gill, A.E. (1982) Atmosphere-Ocean Dynamics, Academic Press, San Diego, 1982.

Graßl, H., V. Jost, R. Kumar, J. Schulz, P. Bauer, and P. Schlüssel (2000) The Hamburg Ocean-Atmosphere Parameters and Fluxes from Satellite Data (HOAPS): A

climatological atlas of satellite derived air-sea-interaction parameters over the oceans, Max Planck Institute for Meteorology, Report No. 312, Hamburg

Grötzner, A., M. Latif, and T. Barnett (1998) A decadal cycle in the North Atlantic Ocean as simulated by the ECHO coupled GCM, *J. Clim.,* **11**, 841-847.

Gordon, A.L. (1986) Interocean exchange of Thermocline Water, *J. Geophys. Res.,* **91C**, 5037-5046.

Kalnay, E., M. Kanamitsu, R. Kistler, W. Collins, M.I. Deaven, L. Gandin, M. Iredell, S. Saha, G. White, J. Woollen, Y. Zhu, M. Chelliah, W. Ebisuzaki, W. Higgins, J. Janowiak, K.C. Mo, C. Ropelewski, A. Leetmaa, R. Reynolds, R. Jenne, and D. Joseph (1996) The NCEP/NCAR 40-year reanalysis project, *Bull. Am. Meteorol. Soc.,* **77**, 437-471.

Kushnir, Y. (1994) Interdecadal variations in North Atlantic sea surface temperature and associated atmospheric conditions. *J. Clim.,* **7**, 141-157.

Lass, H.U., M. Schmidt, V. Mohrholz, and G. Nausch (2000) Hydrographic and current measurements in the area of the Angola-Benguela Front, *J. Phys. Oceanogr.,* **30**, 2589-2609.

Levitus, S., and T. Boyer (1994) World Ocean Atlas 1994, Volume 4: Temperature. NOAA Atlas NESDIS 4, U.S. Department of Commerce, Washington, D.C., 1994.

Niiler, P.P., and E.B. Kraus (1977) One-dimensional models of the upper ocean, in *Modeling and Prediction of the Upper Layers of the Ocean,* edited by E.B. Kraus, pp. 143-172, Pergamon, New York, 1977.

Okumura, Y., S.-P. Xie, A. Numaguti, and Y. Tanimoto (2001) Tropical Atlantic air-sea interaction and its influence on the NAO, *Geophys. Res. Lett.,* **28**, 1507-1510.

Robertson, A.W., and C.R. Mechoso (2000) Interannual and interdecadal variability of the South Atlantic Convergence Zone, *Mon. Weath. Rev.,* **128**, 2947-2957.

Robertson, A.W., C.R. Mechoso, and Y.-J. Kim (2000) The influence of Atlantic sea surface temperature anomalies on the North Atlantic Oscillation, *J. Clim.,* **13**, 122-138.

Ruiz-Barradas, A., J.A. Carton, and S. Nigam (2000) Structure of interannual-to-decadal climate variability in the Tropical Atlantic sector, *J. Clim.* **13**, 3285-3297.

Sterl, A., and A. Kattenberg (1994) Embedding a mixed layer model into an OGCM of the Atlantic: The importance of surface mixing for heat flux and temperature, *J. Geophys. Res.,* **99**, 14,139-14,157.

Sterl, A. (2001a) On the impact of gap-filling algorithms on variability patterns of reconstructed oceanic surface fields, *Geophys. Res. Lett.,* **28**, 2473-2476.

Sterl, A. (2001b) On the impact of gap-filling algorithms on variability patterns of reconstructed oceanic surface fields - an update, *Proceedings of the WCRP/SCOR Workshop on Intercomparison and Validation of Ocean-Atmosphere Flux Fields,* 21-24 May, 2001, Potomac, MD, WMO/TD-No. 1083 (Geneva, 2001), pp 131-134.

Sutton, R.T., S.P. Jewson, and D.P. Rowell (2000) The elements of climate variability in the tropical Atlantic region, *J. Clim.,* **13**, 3261-3284.

Venegas, S.A., L.A. Mysak, and D.N. Straub (1997) Atmosphere-ocean coupled variability in the South Atlantic, *J. Clim.,* **10**, 2904-2920.

Venegas, S.A., L.A. Mysak, and D.N. Straub (1998) An interdecadal climate cycle in the South Atlantic and its links to other ocean basins, *J. Geophys. Res.,* **103C**, 24,723-24,736.

Wainer, I., and S.A. Venegas (2002) South Atlantic multidecadal variability in the Climate System Model, *J. Clim.,* **15**, 1408-1420.

Weijer, W., W.P.M. De Ruijter, A. Sterl, and S.S. Drijfhout (2002) Response of the Atlantic overturning circulation to South Atlantic sources of buoyancy, *Global and Planetary Change,* **34**, 293-311.

Woodruff, S.D., R.J. Slutz, R.L. Jenne, and P.M. Steurer (1987) A Comprehensive Ocean-Atmosphere Data Set, *Bull. Amer. Meteor. Soc.*, **68**, 521-527.

Xie, S.-P., and Y. Tanimoto (1998) A pan-Atlantic decadal climate oscillation, *Geophys. Res. Lett.*, **25**, 2185-2188.

Zebiak, S.A., and M.A. Cane (1987) A model El Niño-Southern Oscillation, *Mon. Weath. Rev.*, **115**, 2262-2278.